Applied Surface Science 638 (2023) 158006

Contents lists available at ScienceDirect

Applied Surface Science

journal homepage: www.elsevier.com/locate/apsusc

Full Length Article

Expeditious and Eco-friendly fabrication of Graphene-Ag nanocomposite for methyl paraben sensing

M. Adeel Zafar [a], Yang Liu [b], Scarlett Allende [a], Mohan V. Jacob [a,*]

[a] Electronics Materials Lab, College of Science and Engineering, James Cook University, Townsville, QLD, 4811, Australia
[b] College of Science and Engineering, James Cook University, Townsville, QLD, 4811, Australia

ARTICLE INFO

Keywords:
Graphene nanosheets
Atmospheric pressure microwave plasma
Electrochemical sensor
Methyl paraben

ABSTRACT

The synthesis of graphene-based nanocomposites using wet chemical techniques entails a number of time-consuming and laborious synthesis stages in addition to the use of potentially dangerous substances. The present article provides a novel approach to green and in-situ synthesis that employs no hazardous chemicals and synthesizes graphene and silver nanoparticles (Ag NPs) nanocomposite from the tea tree oil and silver nitrate ($AgNO_3$) vapours. The synthesis happens in a matter of seconds in microwave plasma at ambient conditions. Images from the scanning and transmission electron microscopy revealed that graphene nanosheets act as the most favoured sites for the Ag NPs to anchor and form a nanocomposite. The investigations revealed a correlation between the concentration of $AgNO_3$ in the precursor and the size and aggregation of Ag NPs. The results of X-ray photoelectron spectroscopy demonstrated a negative shifting of the Ag-doublet, which suggested a strong interaction between Ag NPs and graphene. Additionally, the graphene-Ag nanocomposite drop-casted on screen-printed electrode demonstrated good electrochemical sensing capability for methyl paraben, with a superior linear range of 20 to 260 μM and a commendable limit of detection of 2.5 μM.

1. Introduction

A new class of hybrid materials i.e. graphene-based nanocomposites offers significantly enhanced and multifarious properties. In this regard, various graphene-based nanocomposites comprising different metal oxides and nanoparticles have been developed [1]. The synergy of Ag NPs and graphene nanosheets offered superior properties that have applications in various fields such as catalysis, antimicrobial coatings, sensors etc. [2–5]. Ag NPs composite with pristine graphene, graphene oxide (GO), and reduced-graphene oxide (r-GO) are used in electrochemical sensors [6,7], catalysis [8], biomaterials [9], and chemical detection processes [10]. This promising material, however, still needs attention for its facile and sustainable synthesis.

The production of graphene-Ag nanocomposites has received considerable research interest. Traditional wet chemical methods to synthesize graphene-Ag nanocomposites entail two stages. First, GO is synthesized using the Hummers method, and then it is converted to r-GO or pristine graphene. The Hummers method comprises multiple steps such as stirring, heating, purifying, and drying [8,11]. In the second stage, the composite with Ag is created through another solution-based chemical method, which involves reductants, oxidants, and surfactants [10,12,13]. This two-stage traditional approach is time-consuming and includes the use of hazardous chemicals, which are not only toxic to the environment but also difficult to remove from the nanocomposite. Some of the reductants and surfactants persist as pollutants within the nanocomposite, further affecting the inherent antibacterial activity of the Ag nanoparticles [14]. The use of hazardous compounds at several subsequent phases and laborious synthesis processes are still not addressed, despite attempts by some researchers to investigate green-reducing agents [6,9,15–17].

After successfully implementing microwave plasma for the synthesis of graphene and its derivatives [18–21], researchers began exploring its application in the synthesis of graphene-based nanocomposites. In early studies, as cited [8,22], microwave plasma was utilized to assemble graphene and Ag NPs. In those studies, graphene was synthesized using a wet chemical method that involved the use of strong acids. However, recent advancements have expanded the capabilities of microwave plasma, enabling the synthesis of both graphene and metal nanoparticles simultaneously. For this purpose, a single precursor which contains carbon and metal, for instance, titanium isopropoxide ($C_{12}H_{28}O_4Ti$) is

* Corresponding author at: Electronics Materials Lab, College of Science and Engineering, James Cook University, Townsville, QLD 4811, Australia.
E-mail address: mohan.jacob@jcu.edu.au (M.V. Jacob).

https://doi.org/10.1016/j.apsusc.2023.158006
Received 6 June 2023; Received in revised form 6 July 2023; Accepted 9 July 2023
Available online 10 July 2023

used to synthesize TiO_2-graphene nanocomposite in a single-step [23]. Unfortunately, the requirement of this unique combination of both elements in the same precursor limits the scope of the method to very few nanocomposites. In addition, the technique produces the nanocomposite, which has a fixed amount of metal in the product.

Lately, Jo et al. [24] presented the idea of mixing a metal salt into ethanol and decomposing them in the atmospheric pressure microwave plasma to synthesize Pt-graphene nanocomposite. This approach broadens the choice of metal nanoparticles and gives the freedom to experiment with the proportion of metal and graphene in the nanocomposite. However, not all metal salts fulfil the requirement of the good solubility of metal salt in ethanol. On the other hand, the usage of ethanol vapours above a certain level increases the chances of the plasma undergoing extinction, thereby affecting the overall production rate of the graphene [25]. Dias et al. [18] successfully demonstrated the synthesis of N-graphene-manganese-Oxide/sulphide nanocomposite using microwave plasma. However, the usage of toxic sources, specifically methane/methylamine, in the synthesis raises concerns regarding safety and environmental impact.

There is a high demand for the rapid synthesis of graphene-based nanocomposite using green and sustainable precursors. Herein, we report a facile, dry, and sustainable approach to synthesizing the graphene-Ag nanocomposites using atmospheric pressure microwave plasma (APMP). The APMP method comprises two stages. In the first stage, the graphene is synthesized from a natural source, i.e. tea tree extract, and in the second step, Ag NPs are produced over graphene from $AgNO_3$ vapours. The reasons why APMP is a ground-breaking approach that outperforms all other traditional synthesis methods include: (i) the advantage of reduced synthesis time. Both the graphene and the Ag NPs can be fabricated within just a fraction of a second. (ii) The post-synthesis formalities of washing, drying, etc. are not necessary with this process, nor are any chemicals. Table S1 presents a comparative analysis of the APMP with the previously used methodologies. The APMP offers to use sustainable precursors in milder conditions of plasma (low microwave power, ambient conditions) ensuring that the process is eco-friendly and energy saving. This report also presented the application of as-synthesized graphene-Ag nanocomposite for the detection of methyl paraben (MP), which is an endocrine disruptor chemical.

2. Materials and method

2.1. Raw materials

The essential oil of *melaleuca alternifolia*, commonly known as tea tree was purchased from Australian Botanical Products (ABP, Victoria, Australia). Silver nitrate ($AgNO_3$) and methyl paraben (MP) were procured from Sigma Aldrich, Australia. Lastly, ultrapure water was used to make the solutions.

2.2. Instrumentations

Confocal laser Raman spectroscopy (Witec, 532 nm laser), scanning electron microscopy (SEM) (Hitachi SU 5000), and x-ray photoelectron spectroscopy (XPS) (Kratos Axis Ultra XPS with an Al Kα x-ray source) were used to investigate the structure, morphology, and elemental analysis. X-ray diffraction (XRD) (Bruker, D8-Advance X-ray diffractometer, Cu Kα, $\lambda = 0.154$ nm) was used for crystallographic information. A transmission electron microscope (Hitachi HF5000) was used for transmission electron microscopy (TEM) images. Optical emission spectroscopy was recorded using Avantes equipment.

Electrochemical experimentations were carried out on a PalmSens 4 (Palm Instruments BV, Netherlands) potentiostat. Screen-printed electrodes (SPE) were also purchased from Palm Instruments BV, Netherlands.

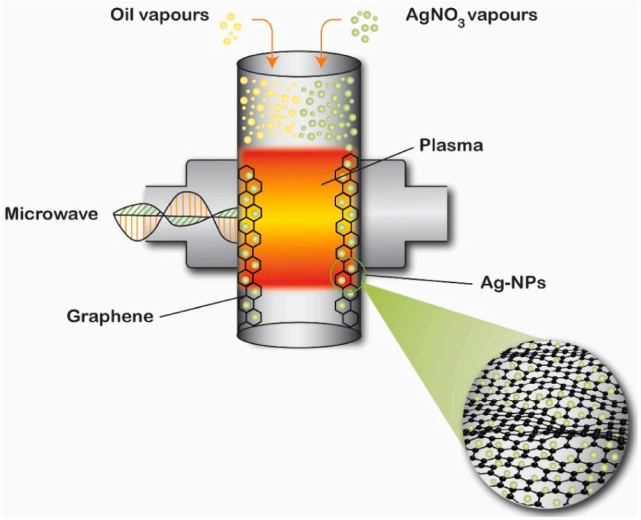

Fig. 1. Schematic illustration of the synthesis of graphene-Ag nanocomposite in atmospheric pressure microwave plasma.

Table 1
Details of synthesis conditions of graphene-Ag nanocomposite.

Factors	Synthesis of graphene	Synthesis of Ag NPs
Precursor	Tea tree essential oil	$AgNO_3$ (0.05 M, 0.10 M, 0.15 M)
Microwave power	250 W	300 W
Argon flow rate	2.5 slm	2.5 slm
Precursor residence time	Few seconds	Few seconds
Synthesis duration	15 min	7 min

2.3. Synthesis of graphene-Ag nanocomposite

Fig. 1 illustrates the synthesis scheme of the graphene-Ag nanocomposite using the APMP. The plasma system composed of a microwave power supply (2.45 GHz), a tuner, a reaction tube made of quartz, and an ultrasonic vaporizer has been used for the experiment. A vaporizer was used to deliver the $AgNO_3$ into the reaction tube as a gas phase, whereas, oil vapours were sent by passing the argon gas through the container carrying tea tree oil.

Table 1 presents the operating condition used for the synthesis. Three different samples, synthesized from different concentrations of $AgNO_3$ i.e. 0.05 M, 0.10 M, and 0.15 M, named 0.05 M graphene-Ag, 0.10 M graphene-Ag, and 0.15 M graphene-Ag were prepared. The synthesis was carried out in two stages. At first, graphene was synthesized on the walls of the quartz tube for 15 min by adding the tea tree oil vapours. After that, the oil supply was stopped and $AgNO_3$ vapours were released for 7 min by switching on the vaporizer. The formation of graphene-Ag nanocomposite (~0.74 mg/min) happened on the walls of the quartz tube. The process has a limitation of non-continuous production due to the single line of precursor supply. Modifying the system to have the ability to provide supplies for both precursors at the same time could enable a continuous production system. As-synthesized graphene-Ag nanocomposite was also collected on Si substrate for evaluation.

2.4. Analytical methods

A disposable screen-printed electrode (SPE) consisting of working, reference, and counter electrodes was used for the electrochemical study. The working electrode (diameter of 3 mm) was modified by drop-casting 5 μL of graphene-Ag nanocomposite followed by drying under room temperature conditions. The modification solution consisted of 1 mg/mL of graphene-Ag nanocomposite in ethanol. The stock solution of

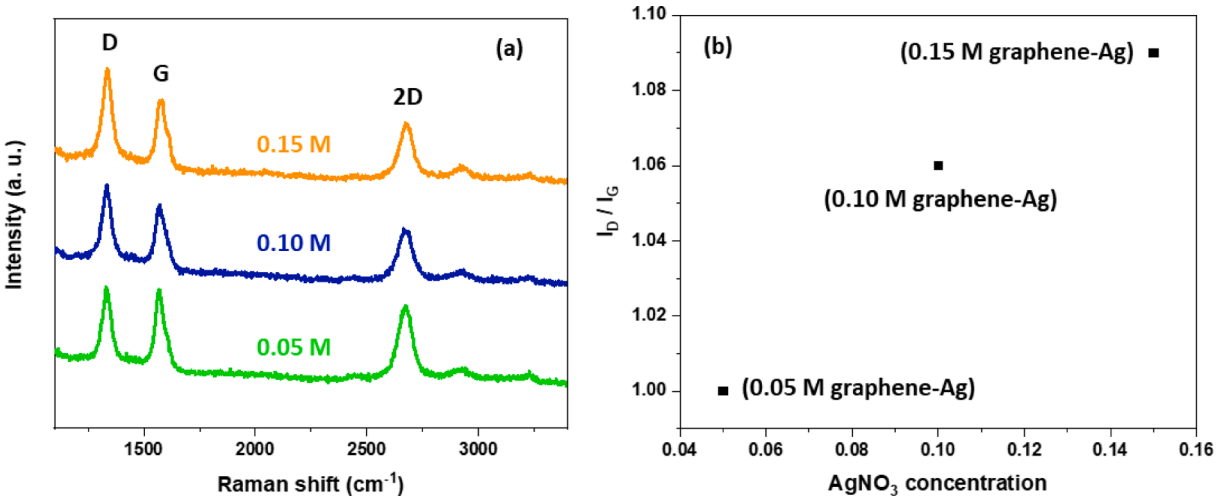

Fig. 2. (a) Raman spectra of graphene-Ag nanocomposites (b) I_D/I_G of graphene-Ag nanocomposites synthesized at different concentrations of $AgNO_3$.

methyl paraben (MP) was prepared in methanol. Cyclic voltammetry and differential pulse voltammetry were used for electrochemical investigations. River water that was gathered from Ross River, Townsville, Australia, was used for real application. Before the experimentation, the river water was treated according to the procedure reported previously [26]. Concisely, the river water was first filtered through a 0.45 μm filter membrane, before it was diluted with 0.1 M PBS (pH 7.01) at a ratio of 1:9. Its pH was reassessed after dilution.

3. Results and discussions

The following results and discussion section provide an in-depth analysis of the characterizations of graphene-Ag nanocomposite. For the characterization of pristine graphene, we recommend referring to a previous study [27] on the synthesis of graphene from tea tree extract. The study provides valuable insights into the properties and characterization techniques relevant to pristine graphene.

3.1. Morphology and structural analysis of graphene-Ag nanocomposite

The Raman spectra of the graphene-Ag nanocomposite samples synthesized at different concentrations of $AgNO_3$ are given in Fig. 2a. The nanocomposites at all concentrations showed prominent D and G peaks along with a signature peak of 2D related to graphene-based materials [28,29].The peak D represents the A_{1g} vibration of the C_6 assembly of atoms appearing after the defects and disorders in the

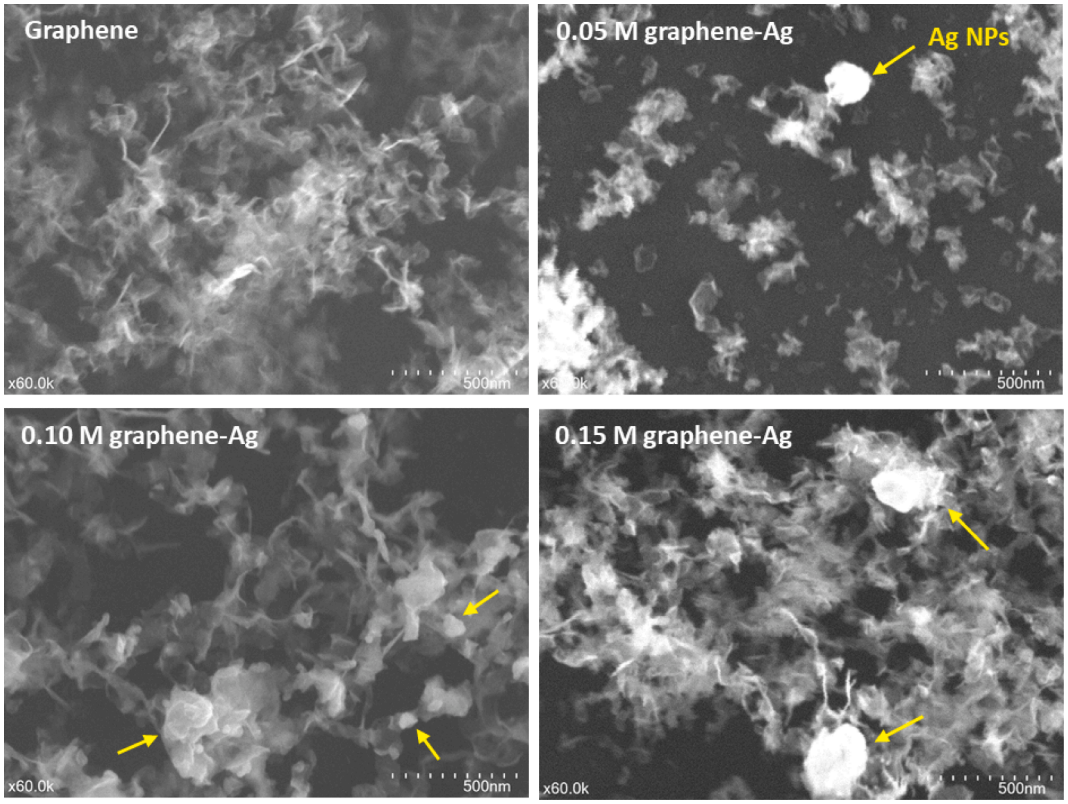

Fig. 3. SEM images of graphene and graphene-Ag nanocomposites synthesized from different concentrations of $AgNO_3$.

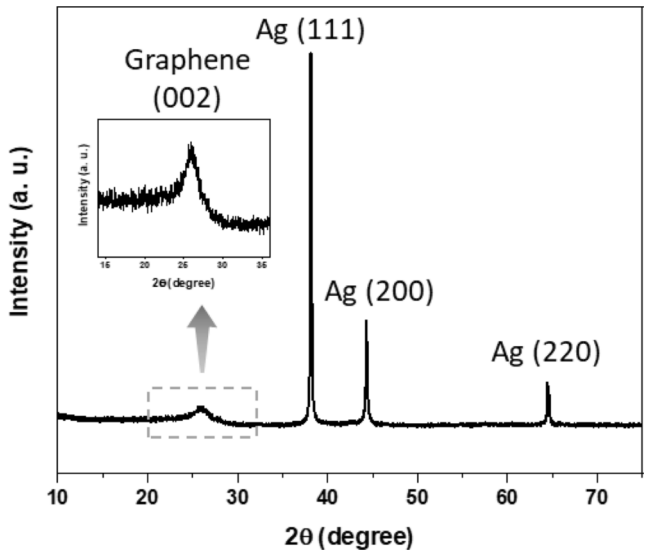

Fig. 4. XRD pattern of 0.10 M graphene-Ag nanocomposite.

structure [30,31]. Additionally, it is also related to the functional groups and doping in the graphene [32,33]. The G peak is attributed to the E_2g vibrational mode of sp^2 carbon [34]. The 2D band is the second order of zone-boundary phonons [35].

Each of the three concentrations had distinct D peaks. This is attributed to the oxygen functional groups found in the graphene's basal plane, which were further validated by XPS. Moreover, Ag NPs might also contribute to these intense D peaks. The degree of imperfection in graphene structure is usually determined by the intensity ratio of the D and G bands [36]. Fig. 2b presents the graph between intensity ratios (I_D/I_G) vs different concentrations of $AgNO_3$. Although negligible differences are found in the values of I_D/I_G, a slight increase with the increase of $AgNO_3$ concentration was found. The number of layers in the graphitic structure may be estimated using full width half maximum (FWHM) along with I_{2D}/I_G [37]. The samples displayed nearly the same FWHM and I_{2D}/I_G values i.e. ~ 59 cm^{-1} and ~ 1.04 respectively. These values are indicative of a few layers of graphene, which has been confirmed through the TEM analysis discussed in the later section.

The structure and morphology of graphene-Ag nanocomposites were investigated using SEM. The SEM images are given in Fig. 3 and Fig. S1 at lower magnification. The images of the samples on Si-substrates showed isolated nanoislands that were amalgamated in a disordered manner. The graphene displayed wrinkled sheet-like morphology similar to that of in the previous reports [38,39]. SEM pictures also show the Ag NPs in close proximity to the graphene nanosheets. The Ag NPs were randomly distributed on the surface of the graphene nanosheets. It appeared that the overall quantity and size of the Ag NPs were affected by the concentration of $AgNO_3$ in the feeding solution. At 0.05 M concentration of $AgNO_3$, the produced amount of Ag NPs was minimal. The 0.10 M concentration of Ag NO_3 showed increased content of the Ag NPs with the varying sizes of the particles. Also, the accumulation of Ag NPs can be observed in the 0.10 M $AgNO_3$ SEM image. However, increased aggregation and the average size of the Ag NPs was observed in case of the 0.15 M graphene-Ag sample. Similar observations have been reported by Yuan et al. [9]. They found that the size and shape of Ag NPs were affected by the varied concentration of $AgNO_3$ precursor.

The 0.10 M graphene-Ag nanocomposite samples were characterized by XRD. The XRD analysis was performed to investigate the crystalline

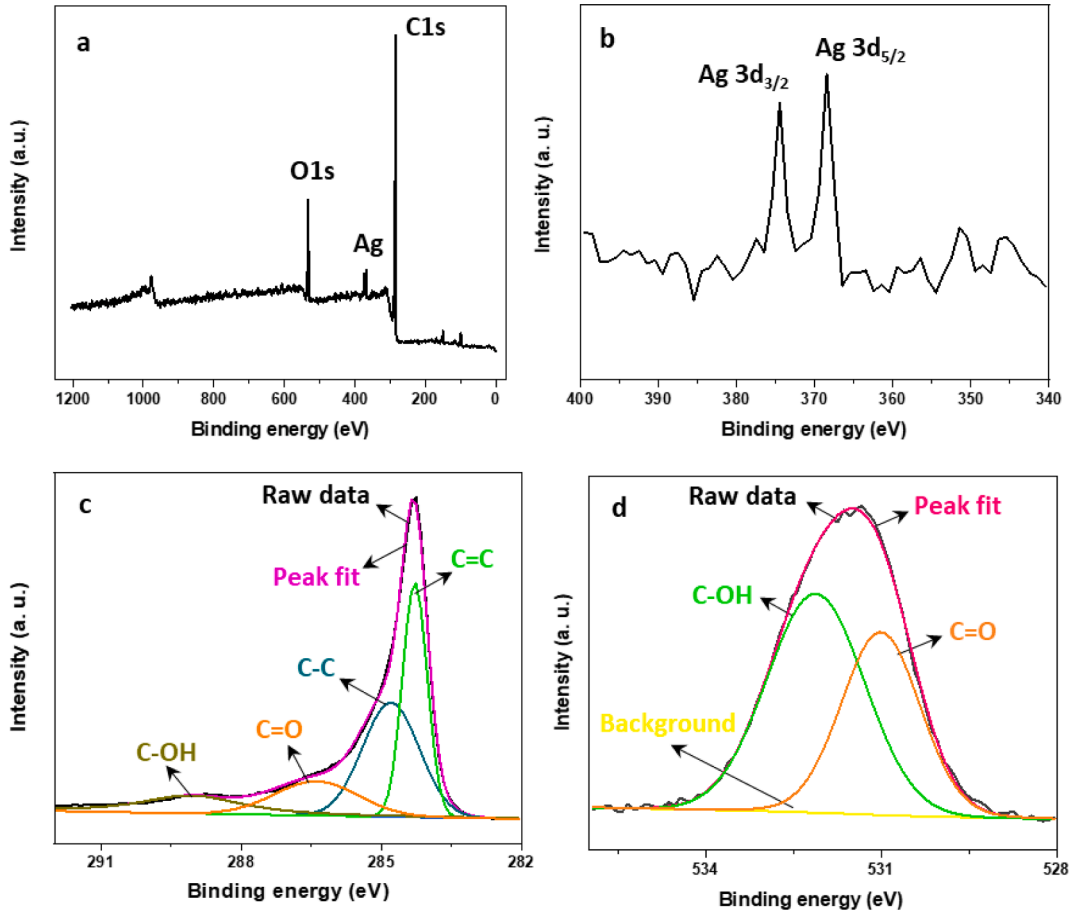

Fig. 5. XPS of (a) 0.10 M graphene-Ag nanocomposite and (b) Ag 3d, High-resolution spectra of (c) C1s and (d) O1s.

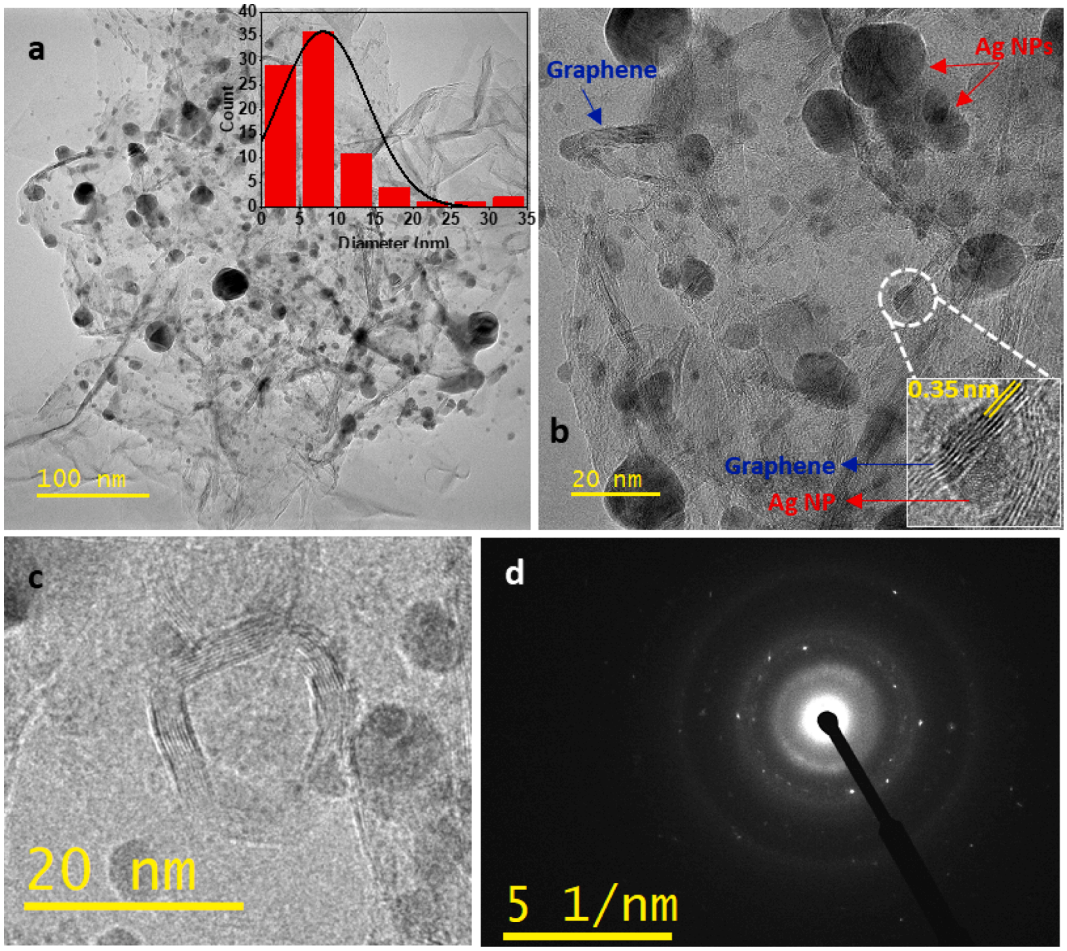

Fig. 6. TEM images of 0.10 M graphene-Ag nanocomposite at (a) lower and (b) higher magnification (c) TEM image of carbon nano-onion (d) SAED pattern of 0.10 M graphene-Ag nanocomposite. Inset in the image (a) represents the corresponding particle size distribution.

nature of the material. The XRD pattern given in Fig. 4 exhibited four peaks. The characteristic peak of graphene (magnified in the inset image) can be observed at a 2θ value of 25.8° corresponding to the (0 0 2) plane [40]. The interlayer spacing of 0.34 nm, calculated through Bragg's law, roughly matches the value of the same in TEM results. The distinctive peaks at 38.14°, 44.36°, and 64.5° corresponding to (1 1 1), (2 0 0), and (2 2 0) planes respectively, are ascribed to the crystalline planes of Ag NPs [3].

The 0.10 M graphene-Ag nanocomposite sample was subjected to XPS analysis in order to reveal the elemental composition and functional group species. The survey scan XPS of pristine graphene presented in Fig. S2 showed the presence of carbon (C) and oxygen (O); whereas the XPS of 0.10 M graphene-Ag nanocomposite in Fig. 5a revealed silver (Ag) beside the C and O, centred at 284.2, 531.5, and 370 eV respectively. The compositions of the C, O, and Ag elements were found as ~ 86, ~8, and 6 % respectively. High-resolution spectra of C1s, O1s, and Ag were also analysed to investigate the bonding structure.

C1s high-resolution spectrum was deconvoluted into its respective peaks. It is given in Fig. 5c. The deconvolution discovered four component peaks. The main C = C peak related to sp^2-C which appeared at 248.4 eV, is a signature of graphene material. In addition, the structure contained C–C (sp^3-C), C = O, and C-OH located at 285.1, 286.3, and 289.1 eV respectively. The presence of sp^2-C is indicative of the honeycomb lattice structure of graphene. Whereas, the sp^3-C peak was attributed to the edges of the graphene or the substitutional defects in the structure [41]. The O1s, given in Fig. 5d demonstrated contributions from C = O and C-OH peaks at 531 and 532 eV respectively.

A magnified image of the XPS of the Ag 3d in Fig. 5b revealed the doublet of the Ag NPs. Ag $3d_{5/2}$ and Ag $3d_{3/2}$ were allocated to the peaks with centres at 367.9 and 374 eV, respectively. When compared to the typical peaks for Ag metal at 368.2 and 374.2 eV, these peaks are located at lower binding energies [42]. Similar findings were made in earlier research, where the negative shifting was attributed to the transport of electrons from metallic Ag to the graphene sheets as well as an interaction between the Ag and the carboxylic groups (C = O) in the graphene structure [8,43].

Additionally, TEM was used to characterize the 0.10 M graphene-Ag nanocomposite. A low-resolution TEM image shown in Fig. 6a displays graphene nanosheets well-loaded with Ag NPs. The graphene is made up of a few to several layers of folded and wrinkled sheets. The interlayer gap of 0.35 nm was observed, and this value almost matches the one determined by employing XRD. An interesting feature of carbon nano-onion shown in Fig. 6c, was also observed in the TEM images. The carbon nano-onions are pentagonal or quasi-spherical-shaped concentric graphitic layers. These are regarded as a precursor to graphene [44].

Heterogeneous distribution of Ag NPs on graphene nanosheets has been observed in Fig. 6a. The Ag NPs are spherical and have varying sizes ranging between a few nanometres to 60 nm. The size distribution histogram of Ag NPs is acquired by measuring the sizes of 84 randomly selected particles from the corresponding TEM image shown in Fig. 6a. The analysis reveals that the mean size of the Ag NPs is approximately 8 nm. This information is depicted in the inset of Fig. 6a. A high-resolution image in Fig. 6b shows that most of the Ag NPs are well embedded with the graphene nanosheets. A magnified inset image in Fig. 6b displays the implantation of the Ag nanoparticle into graphene. This finding shows that graphene is a preferred location for Ag NPs to accumulate and form

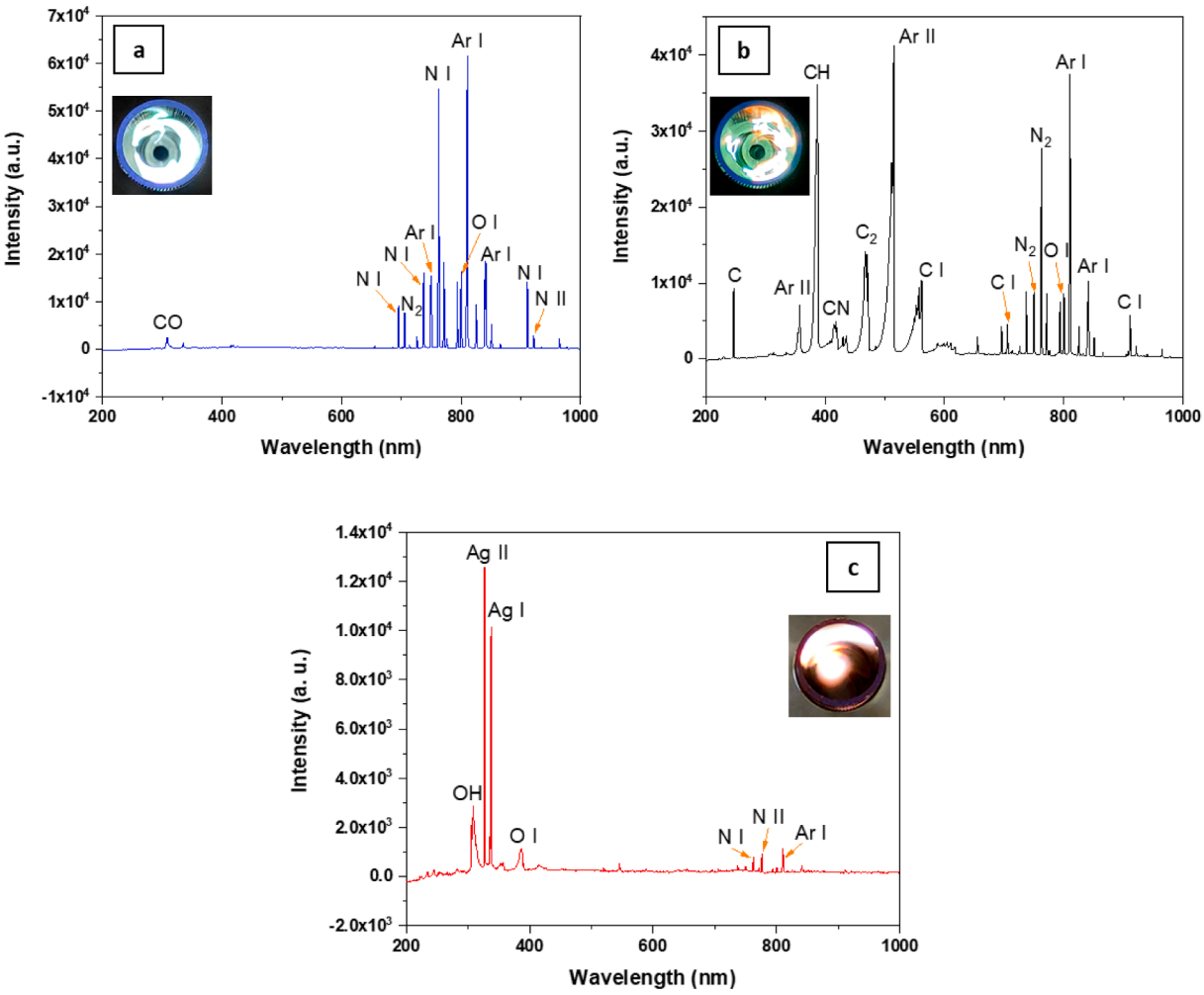

Fig. 7. OES spectra of (a) pure Ar (b) Ar with tea tree oil vapours and (c) Ar with 0.1 M $AgNO_3$ vapours.

a robust connection. This phenomenon also advocates the shifting of the Ag doublet to lower binding energies (XPS Fig. 5b), where it was attributed to the electron transfer from Ag to graphene and/or interaction between the Ag and the carboxylic groups (C = O) in the graphene structure. The large and thick dark nanoparticles are due to the aggregation of smaller Ag NPs. The particle size and aggregation are more in the 0.15 M $AgNO_3$ sample due to the higher concentration of $AgNO_3$ in the solution. It is shown in Fig. S3. The SAED pattern presented in Fig. 6d demonstrates the characteristic rings for the (111), (200), and (220) planes of the face-centred cubic Ag structure.

3.2. Optical emission spectroscopy measurements

Optical emission spectroscopy (OES) was used to determine the light-emitting species by pointing the optical fibre to the plasma through a viewing window. The images of the plasma and OES spectrums were recorded by using three distinct states of plasma, i.e. pure Ar plasma (Fig. 7a), Ar plasma with tea tree oil vapours (Fig. 7b), and Ar plasma with 0.1 M $AgNO_3$ vapours (Fig. 7c). The images of the plasma displaying unique colours are given in the insets of respective figures. The pure Ar plasma, generated at 250 W microwave power, mainly consisted of colourless strikes with some shades of sea green colour. Atomic Ar and nitrogen (N) dominated the OES spectra. The atmospheric circumstances of the synthesis were responsible for the presence of N and a little amount of oxygen (O) in the plasma. A low-intensity peak of carbon monoxide (CO) at a lower wavelength was also observed in the spectrum. The primary components of the OES spectra of pure Ar plasma measured by Melero et al. [45] at 300 W microwave power and atmospheric conditions were also Ar and N. However, contrary to our observations, they pointed out that most N exists as molecules bound to O, C, and H. This dissimilarity can be attributed to the different amounts of the elements present in the precursors used for the synthesis.

The tea tree oil vapours in the Ar plasma (operated at 250 W microwave power) showed an orange colour appearing in some parts of the plasma. The orange colour provide evidence of the occurrence of decomposition of oil vapours and graphene formation in the plasma. Despite using tea tree to form graphene, the species created were comparable to those described in the prior research on the OES spectrum where they used ethanol for this purpose [38]. The OES spectrum showed a significant contribution of C in atomic as well as molecular form. The carbon peaks mainly appeared at lower wavelengths ranging between 248 and 720 nm. The dominant species in the spectrum is C_2, which was formerly thought to be a precursor in the creation of graphene. Its existence in the spectrum is viewed as evidence that graphene was formed because of it [46,47]. In comparison with pure Ar plasma, the decline in peak intensities of Ar and N emissions was observed. It has been previously reported that the drop in the intensity happens due to the consumption of part of the supplied energy in the dissociation of precursor i.e. oil vapours [45].

In the case of Ar plasma with 0.1 M $AgNO_3$ vapours (operated at 300 W), two strong bands of Ag near 300 nm wavelength can be observed. Other bands i.e. N and Ar have drastically descended. It suggests that the environment of the plasma was considerably different from pure Ar or Ar with oil vapours plasma. The image of the plasma shown in the inset

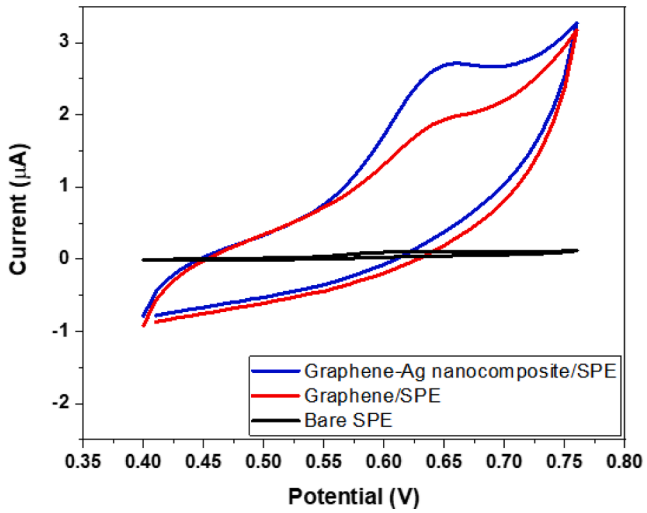

Fig. 8. Cyclic voltammograms of (a) bare SPE, (b) graphene/SPE, (c) graphene-Ag nanocomposite/SPE in 0.1 M PBS (pH 7.01) containing 10 μM MP.

of Fig. 7c also showed comparatively different colours and mainly consisted of golden and purple colours. Since the $AgNO_3$ solution was made using distilled water, there are many water molecules in the vapors that were supplied into the tube. These vapours produced the OH peak at ~ 308 nm in the OES spectrum. The observation of the Ag peaks were in good accord with the previous findings, although they also found additional peaks of atomic Ag at longer wavelengths (850 nm) [48]. However, their method of synthesis seems to be distinct in that they employed Ag electrodes to create Ag NPs rather than vapours to make them.

3.3. Electrochemical detection of methyl paraben

Cyclic voltammetry (CV) is a very useful electrochemical practice for investigating redox reactions at the interface of solution and electrode. The cyclic voltammetry (CV) technique was used to investigate the electrochemical behaviour of MP at the bare SPE, graphene/SPE, and graphene-Ag nanocomposite/SPE. The bare SPE, scanned in 0.1 M PBS (pH 7.01) containing 10 μM MP, showed an oxidation peak around 0.64 V with a peak current of a small value of 0.1 μA (Fig. 8). The graphene/SPE showed an enhanced peak current value of ~ 0.5 μA, which increased to ~ 1.4 μA in the case of graphene-Ag nanocomposite/SPE. They are shown in Fig. 8. Due to the irreversible nature of the process [49,50], no reduction peaks were observed.

Differential pulse voltammetry (DPV) was used to obtain the linear range of the calibration curve at the graphene-Ag nanocomposite/SPE sensor. The successive addition of MP into the solution showed an increased oxidation peak current. The voltammograms are presented in Fig. 9a. The measured peak currents were plotted against the concentration of MP to find the calibration curve. As displayed in Fig. 9b, the peak currents were linear in the range from 20 to 260 μM, where the linear regression equation is $y = 0.03385x + 6.0757$ ($R^2 = 0.995$). The increase in concentration beyond 260 μM showed only a slight rise in peak current, which resulted in the deviation of the curve from linearity. The limit of detection (LOD) of 2.5 μM was determined by identifying the smallest amount the sensor can detect. Table 2 shows a comparative overview of our results with the past works. It can be noted that the proposed sensor showed wide linear range and commendable LOD.

3.3.1. Repeatability, reproducibility, and stability of the sensor

The repeatability study, which is an important analytical performance, was investigated using one modified graphene-Ag nanocomposite/SPE electrode for five consecutive measurements. The peak current values are shown in Fig. 10a. The relative standard deviation (RSD) was calculated as 3.98 %. The recorded DPV curves are given in Fig. S4. The reproducibility of the electrode was investigated by preparing five different graphene-Ag nanocomposite/SPE electrodes. The peak current values against electrode number are presented in Fig. 10b. The obtained DPV curves displayed in Fig. S5 gave an RSD of 5.13 % which was comparable with the value given in the literature [53]. Furthermore, the stability test was conducted by storing graphene-Ag

Table 2
Comparison of electrochemical performance of sensor for methyl paraben detection.

Electrode	Method	Linear range (μM)	Limit of detection (μM)	References
AuNP/RGO/CS/GCE	SWV	0.03—1.3	0.0138	[51]
RGO/RuNPs/GCE	DPV	0.5—3	0.24	[52]
PoL/RGO/GCE	DPV	1—200	0.2	[53]
ZnO/GCE	SWV	20—120	7.25	[54]
MWCNTs/LB/GCE	LSV	1—80	0.4	[55]
MWCNTs/Hb/CPE	DPV	0.1—13	0.025	[56]
Au/$(MNP/Ppy)_3$	DPV	0.0—131.4	0.09	[57]
graphene-Ag/SPE	DPV	20—260	2.5	This work

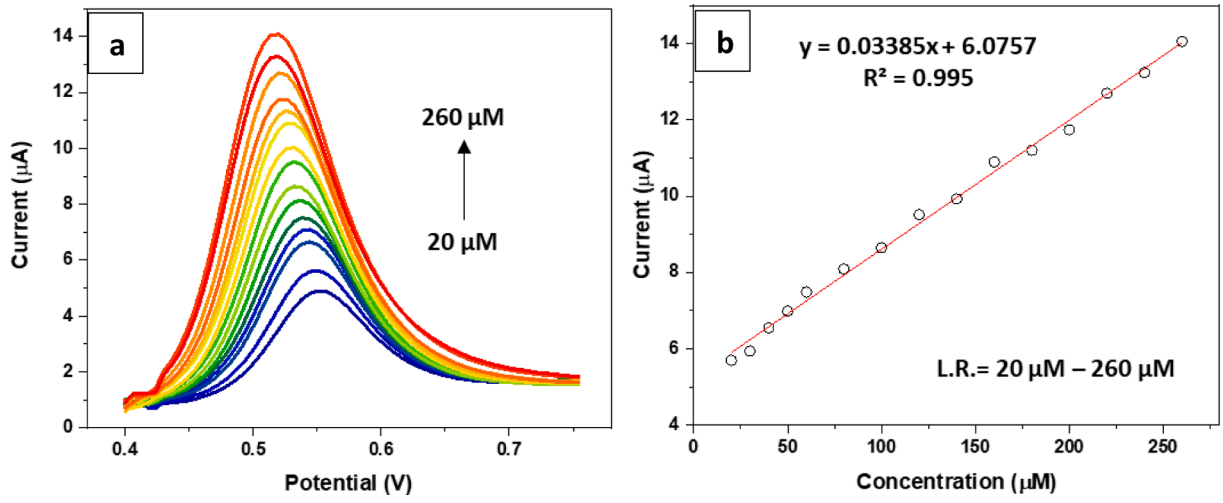

Fig. 9. (a) Differential pulse voltammogramms of different concentrations of MP (20, 30, 40, 50, 60, 80, 100, 120, 140, 160, 180, 200, 220, 240, 260 μM) in 0.1 M PBS (pH 7.01) and **(b)** corresponding calibration curve.

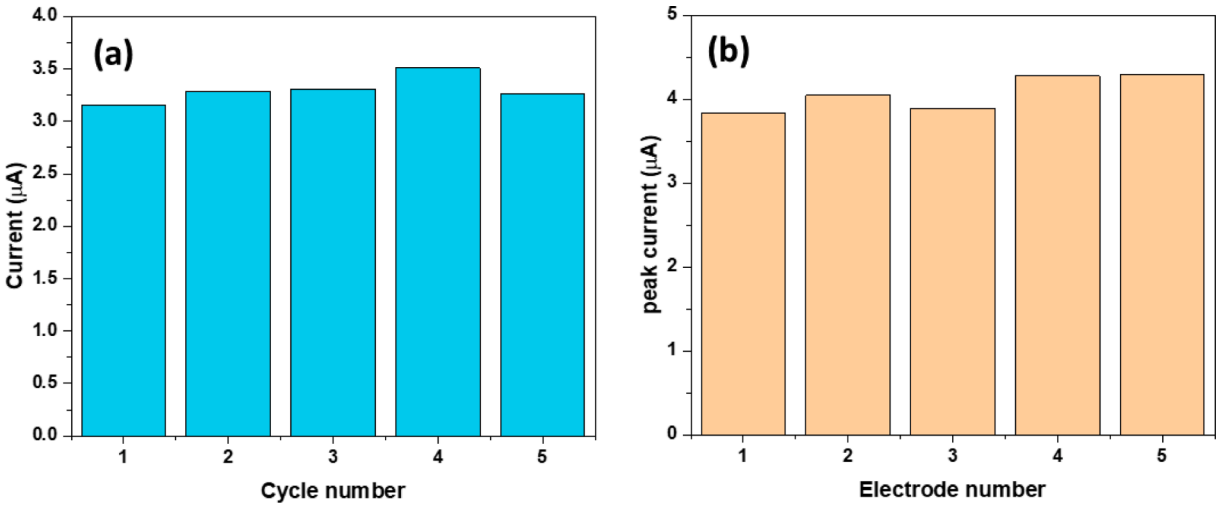

Fig. 10. (a) Repeatability study of one graphene-Ag nanocomposite/SPE in 0.1 M PBS containing 20 μM MP. **(b)** Reproducibility study of five graphene-Ag nanocomposite/SPEs in 0.1 M PBS containing 20 μM MP.

nanocomposite/SPE electrode in a closed container for two weeks, which indicated that the current response retained 95 % of the initial value. The corresponding DPV curves are shown in Fig. S6.

3.3.2. *Selectivity of the sensor*

The selectivity of graphene-Ag nanocomposite towards MP with interferents (oxalic acid, sodium nitrate, sodium nitrite, diuron and paraquat) was investigated. These interferents were chosen due to their potential coexistence in real samples. For this purpose, a mixture of MP and its interferents (20 μM each) was prepared in 0.1 M PBS (pH 7.01). The DPV curves of MP and its mixture with interferents are shown in Fig. S7. It was evident that the interferents had no impact on the MP signal. The sensor retained its remarkable MP selectivity even in the replicates.

3.3.3. *Real sample analysis*

The applicability of graphene-Ag nanocomposite/SPE for the analysis of real samples was demonstrated by investigating the recoveries for the MP determination in river water. As shown in Fig. S6, upon the addition of 20 μM MP in river water, a prominent current response was observed. Whereas, the blank river water displayed no current peak. The corresponding DPV curves are shown in Fig. S8. The recovery value of 93 % makes the proposed sensor suitable for real application. In comparison with 0.1 M PBS (pH 7) containing 20 μM MP, the peak potential in river water slightly shifted from 0.55 V to a lower potential of 0.54 V. It can be attributed to the lower pH noted for river water i.e. 6.92.

4. Conclusion

A rapid and environmentally benign approach for synthesizing graphene-Ag nanocomposite was reported in this work. The nanocomposite was synthesized inside the atmospheric pressure microwave plasma by virtue of tea tree extract and $AgNO_3$ vapour dissociation. The formation of the nanocomposite was confirmed by XRD, which showed signature peaks related to the graphene and Ag materials. The OES spectrum recorded during the synthesis of pristine graphene showed atomic and molecular bands of C, particularly C_2 which were deemed as the precursor for graphene synthesis. Whereas, the OES spectrum of pure Ar plasma, and Ar with $AgNO_3$ vapours were mainly dominated by Ar and N, and Ag species respectively. A strong interaction between graphene and Ag NPs was depicted in XPS spectrum, which showed a slight shift of Ag-doublet (Ag $3d_{5/2}$ and Ag $3d_{3/2}$) towards lower binding energies. The TEM images also revealed good embedment of Ag NPs with the graphene nanosheets. Interestingly, the concentration of $AgNO_3$ played a pivotal role in the determination of the size and aggregation of Ag NPs. Based on the results observed in this work, the $AgNO_3$ concentration of 0.1 M was proposed as an optimum value for well-dispersed and nano-size Ag NPs. They are imperative for high electrocatalytic activity of graphene. The usage of graphene-Ag nanocomposite in the electrochemical detection of harmful methyl paraben showed a limit of detection of 2.5 μM and a linear range of 20 to 260 μM, which are superior to some of the results reported earlier.

CRediT authorship contribution statement

M. Adeel Zafar: Methodology, Investigation, Formal analysis, Conceptualization, Data curation, Project administration, Writing – original draft. **Yang Liu:** Supervision, Formal analysis, Writing – review & editing. **Scarlett Allende:** Validation, Visualization. **Mohan V. Jacob:** Methodology, Supervision, Funding acquisition, Formal analysis, Project administration, Writing – review & editing.

Declaration of Competing Interest

The authors declare that they have no known competing financial interests or personal relationships that could have appeared to influence the work reported in this paper.

Data availability

Data will be made available on request.

Acknowledgment

M.A.Z. gratefully acknowledges financial support provided by James Cook University through the International Research Training Program Scholarship (IRTPS). The authors thank the Centre for Microscopy and Microanalysis (CMM), the University of Queensland for providing facilities for XPS, XRD, and TEM analysis.

Appendix A. Supplementary data

Supplementary data to this article can be found online at https://doi.org/10.1016/j.apsusc.2023.158006.

References

[1] T.A. Saleh, G. Fadillah, Recent trends in the design of chemical sensors based on graphene–metal oxide nanocomposites for the analysis of toxic species and biomolecules, TrAC Trends Anal. Chem. 120 (2019), 115660.
[2] K. Garg, et al., Preparation of graphene nanocomposites from aqueous silver nitrate using graphene oxide's peroxidase-like and carbocatalytic properties, Sci. Rep. 10 (1) (2020) 1–13.
[3] C. Krishnaraj, et al., Silver nanoparticles decorated reduced graphene oxide: Eco-friendly synthesis, characterization, biological activities and embryo toxicity studies, Environ. Res. 210 (2022) 112864.
[4] C.M. Kurmarayuni, et al., Sustainable synthesis of silver decorated graphene nanocomposite with potential antioxidant and antibacterial properties, Mater. Lett. 308 (2022) 131116.
[5] R. Ghanbari, et al., Graphene decorated with silver nanoparticles as a low-temperature methane gas sensor, ACS Appl. Mater. Interfaces 11 (24) (2019) 21795–21806.
[6] K.-J. Peng, et al., Hydrogen-free PECVD growth of few-layer graphene on an ultra-thin nickel film at the threshold dissolution temperature, J. Mater. Chem. C 1 (24) (2013) 3862–3870.
[7] X. Zhao, et al., Monodispersed and spherical silver nanoparticles/graphene nanocomposites from gamma-ray assisted in-situ synthesis for nitrite electrochemical sensing, Electrochim. Acta 295 (2019) 434–443.
[8] K.-C. Hsu, D.-H. Chen, Green synthesis and synergistic catalytic effect ofAg/reduced graphene oxide nanocomposite, Nanoscale Res. Lett. 9 (1) (2014) 1–10.
[9] W. Yuan, Y. Gu, L. Li, Green synthesis of graphene/Ag nanocomposites, Appl. Surf. Sci. 261 (2012) 753–758.
[10] A. Aziz, et al., Silver/graphene nanocomposite-modified optical fiber sensor platform for ethanol detection in water medium, Sens. Actuators B 206 (2015) 119–125.
[11] J. Chen, et al., An improved Hummers method for eco-friendly synthesis of graphene oxide, Carbon 64 (2013) 225–229.
[12] Y. Guo, et al., Reduced graphene oxide heterostructured silver nanoparticles significantly enhanced thermal conductivities in hot-pressed electrospun polyimide nanocomposites, ACS Appl. Mater. Interfaces 11 (28) (2019) 25465–25473.
[13] Z. Xu, H. Gao, H. Guoxin, Solution-based synthesis and characterization of a silver nanoparticle–graphene hybrid film, Carbon 49 (14) (2011) 4731–4738.
[14] M.A. Ahmad, et al., Synergistic antibacterial activity of surfactant free Ag–GO nanocomposites, Sci. Rep. 11 (1) (2021) 196.
[15] Z. Zhang, et al., A facile one-pot method to high-quality Ag-graphene composite nanosheets for efficient surface-enhanced Raman scattering, Chem. Commun. 47 (22) (2011) 6440–6442.
[16] X.-Z. Tang, et al., Growth of silver nanocrystals on graphene by simultaneous reduction of graphene oxide and silver ions with a rapid and efficient one-step approach, Chem. Commun. 47 (11) (2011) 3084–3086.
[17] Z. Çiplak, N. Yildiz, A. Çalimli, Investigation of graphene/Ag nanocomposites synthesis parameters for two different synthesis methods, Fullerenes, Nanotubes, Carbon Nanostruct. 23 (4) (2015) 361–370.
[18] A. Dias, et al., N-graphene-metal-oxide(sulfide) hybrid nanostructures: Single-step plasma-enabled approach for energy storage applications, Chem. Eng. J. 430 (2022) 133153.
[19] P. Fortugno, et al., Synthesis of freestanding few-layer graphene in microwave plasma: The role of oxygen, Carbon 186 (2022) 560–573.
[20] O. Jašek, et al., Study of graphene layer growth on dielectric substrate in microwave plasma torch at atmospheric pressure, Diam. Relat. Mater. 105 (2020) 107798.
[21] A. Dato, Graphene synthesized in atmospheric plasmas—A review, J. Mater. Res. 34 (1) (2019) 214–230.
[22] Y. Wei, et al., Dry plasma synthesis of graphene oxide–Ag nanocomposites: A simple and green approach, Mater. Res. Bull. 53 (2014) 145–150.
[23] U.S. Heo, et al., A facile synthesis of anatase TiO_2-Graphene nanocomposites using plasma and heat treatment, Appl. Surf. Sci. 474 (2019) 118–126.
[24] E.H. Jo, et al., One-step synthesis of Pt/graphene composites from Pt acid dissolved ethanol via microwave plasma spray pyrolysis, Sci. Rep. 6 (1) (2016) 1–8.
[25] M. Jimenez, et al., Hydrogen production from ethanol decomposition by a microwave plasma: Influence of the plasma gas flow, Int. J. Hydrogen Energy 38 (21) (2013) 8708–8719.
[26] P. Xiao, et al., An Fe-MOF/MXene-based ultra-sensitive electrochemical sensor for arsenic (III) measurement, J. Electroanal. Chem. 916 (2022) 116382.
[27] M.A. Zafar, et al., Plasma-Based synthesis of freestanding graphene from a natural resource for sensing application, Adv. Mater. Interfaces 10 (11) (2023) 2202399.
[28] M.A. Zafar, M.V. Jacob, Synthesis of free-standing graphene in atmospheric pressure microwave plasma for the oil-water separation application, Appl. Surf. Sci. Adv. 11 (2022) 100312.
[29] M.S. Kamel, C.T. Stoppiello, M.V. Jacob, Single-step, catalyst-free, and green synthesis of graphene transparent electrode for organic photovoltaics, Carbon 202 (2023) 150–158.
[30] J. Liu, et al., Graphitic carbon nitride (g-C_3N_4)-derived N-rich graphene with tuneable interlayer distance as a high-rate anode for sodium-ion batteries, Adv. Mater. 31 (24) (2019) 1901261.
[31] M.A. Zafar, et al., Plasma-based synthesis of freestanding graphene from a natural resource for sensing application, Adv. Mater.Interfaces (2023) 2202399.
[32] M.A. Zafar, et al., Single-step synthesis of nitrogen-doped graphene oxide from aniline at ambient conditions, ACS Appl. Mater. Interfaces (2022).
[33] M.A. Zafar, et al., Electrochemical sensing of oxalic acid using silver nanoparticles loaded nitrogen-doped graphene oxide, Carbon Trends 8 (2022) 100188.
[34] A.D. Pingale, et al., Facile synthesis of graphene by ultrasonic-assisted electrochemical exfoliation of graphite, Mater. Today:. Proc. 44 (2021) 467–472.
[35] X. Kong, et al., Synthesis of graphene-like carbon from biomass pyrolysis and its applications, Chem. Eng. J. 399 (2020) 125808.
[36] A. Eckmann, et al., Probing the nature of defects in graphene by Raman spectroscopy, Nano Lett. 12 (8) (2012) 3925–3930.
[37] A. do Nascimento Barbosa, et al., Direct synthesis and characterization of graphene layers on silica glass substrates, Mater. Today:. Proc. 10 (2019) 400–407.
[38] J. Toman, et al., On the transition of reaction pathway during microwave plasma gas-phase synthesis of graphene nanosheets: From amorphous to highly crystalline structure, Plasma Processes Polym. (2021) e2100008.
[39] N. Bundaleska, et al., Prospects for microwave plasma synthesized N-graphene in secondary electron emission mitigation applications, Sci. Rep. 10 (1) (2020) 1–13.
[40] T.T. Baby, S. Ramaprabhu, Synthesis and nanofluid application of silver nanoparticles decorated graphene, J. Mater. Chem. 21 (26) (2011) 9702–9709.
[41] R. Al-Gaashani, et al., XPS and structural studies of high quality graphene oxide and reduced graphene oxide prepared by different chemical oxidation methods, Ceram. Int. 45 (11) (2019) 14439–14448.
[42] R. Nair, et al., Unimpeded permeation of water through helium-leak–tight graphene-based membranes, Science 335 (6067) (2012) 442–444.
[43] H. Hu, et al., Preparation and properties of graphene nanosheets–polystyrene nanocomposites via in situ emulsion polymerization, Chem. Phys. Lett. 484 (4) (2010) 247–253.
[44] S. Alancherry, et al., Fabrication of nano-onion-structured graphene films from citrus sinensis extract and their wetting and sensing characteristics, ACS Appl. Mater. Interfaces (2020).
[45] C. Melero, et al., Scalable graphene production from ethanol decomposition by microwave argon plasma torch, Plasma Phys. Controlled Fusion 60 (1) (2017) 014009.
[46] A. Dato, M. Frenklach, Substrate-free microwave synthesis of graphene: Experimental conditions and hydrocarbon precursors, New J. Phys. 12 (12) (2010) 125013.
[47] M.A. Zafar, M.V. Jacob, Plasma-based synthesis of graphene and applications: A focused review, Rev. Mod. Plasma Phys. 6 (1) (2022) 1–38.
[48] I.N.D. Ocampo, G.M. Malapit, R.Q. Baculi, Ar/O_2 atmospheric pressure plasma jet treatment of pure cotton fabric for antibacterial application, Plasma Fusion Res. 13 (2018) 3406116.
[49] S. Michalkiewicz, Anodic oxidation of parabens in acetic acid–acetonitrile solutions, J. Appl. Electrochem. 43 (1) (2013) 85–97.
[50] M. Hasanzadeh, et al., Electrocatalytic oxidation of selected parabens on zinc hydroxide nanoparticles, Catal. Commun. 19 (2012) 10–16.
[51] J.V. Piovesan, E.R. Santana, A. Spinelli, Reduced graphene oxide/gold nanoparticles nanocomposite-modified glassy carbon electrode for determination of endocrine disruptor methylparaben, J. Electroanal. Chem. 813 (2018) 163–170.
[52] C.D. Mendonça, et al., Methylparaben quantification via electrochemical sensor based on reduced graphene oxide decorated with ruthenium nanoparticles, Sens. Actuators B 251 (2017) 739–745.
[53] T.T.T. Toan, Detection of methylparaben in cosmetics by poly L-Lysine/reduced graphene oxide-based sensor, ECS Sensors Plus 1 (3) (2022) 031603.
[54] S. Javaid, et al., Zinc oxide nanoparticles as antifouling materials for the electrochemical detection of methylparaben, ChemElectroChem 8 (1) (2021) 187–194.
[55] L. Wang, et al., A new strategy for enhancing electrochemical sensing from MWCNTs modified electrode with Langmuir-Blodgett film and used in determination of methylparaben, Sens. Actuators B 211 (2015) 332–338.
[56] A. Hajian, et al., Nanomolar detection of methylparaben by a cost-effective hemoglobin-based biosensor, Mater. Sci. Eng. C 69 (2016) 122–127.
[57] L.F. de Lima, et al., Layer-by-Layer nanostructured films of magnetite nanoparticles and polypyrrole towards synergistic effect on methylparaben electrochemical detection, Appl. Surf. Sci. 505 (2020) 144278.